# Isotopic investigation of venting $CO_2$ from a subsurface source

*$CO_2$ venting in the atmosphere through surface waters with fringing bacterial discoloration*

Internship Report & Msc. Thesis

Bob Mulder
Student#: 3345890
Msc. Student Earth, Life & Climate
Utrecht University
Supervisors: T.V. Goldberg (TNO) & M.Ziegler (UU) M.E.G. Hofmann (former UU)

15-10-2017

**Table of contents:**

## 1.Abstract

With this research, measuring the clumped signal on δ47 for $CO_2$ samples obtained from naturally leaking subsurface sources in central Italy is investigated for its viability to identify the possible temperature and hence depth of the source of origin by applying a geothermal gradient. The δ47 clumped signal can be linked to specific temperature ranges, which can be transformed to depth by applying a geothermal gradient to the calculated temperature range, solving for depth. This research investigates methods of cryogenic $CO_2$ purification processing to measure the δ47 clumped isotopic signal of a sampled $CO_2$ gas. On a dual inlet mass spectrometer (IRMS). Whether $CO_2$'s δ47 clumped signal can be used to derive the depth of the subsurface source of origin, depends on the upwards $CO_2$ migration flux through a permeable, porous succession vs. the chemical equilibration reaction speed between $CO_2$ and (ground)water. The D47 Clumped signal is deemed to be independent of variable groundwater geochemistry (Affek, 2013), and in systems containing CO2 vapor and liquid water, dissolution of carbon dioxide is the rate-limiting step (Clog et al., 2015). Using Δ47 as an indicator of the source of depth might be held to a certain limited, since the equilibration speed with water (reactions 2 & 3) could be very high considering the observed trend of increasing equilibration reaction speeds. For the purpose of mitigating hazardous conditions concerning onshore CCS by using Δ47 as an indicator to monitor for subsurface $CO_2$ leakage, is doubtful to be a reliable application. This hypothesis is made on the extrapolation of the observed trend of Clog et al., (2015)'s results concerning an increasing isotopologue exchange rate for Δ47 at increasing temperatures in low temperature ranges. This hypothesis could not be confirmed nor denied by the performed IRMS measurements for δ47 of the sampled $CO_2$ gases.

## 2.Introduction

The ENOS project (ENabling Onshore $CO_2$ Storage in Europe) has been initiated to (1) increase field experience relevant to geological storage of $CO_2$, (2) refine techniques and tools used for site selection and monitoring and (3) to advance communication between science and society on the geological storage of $CO_2$. ENOS is an initiative of $CO_2$ GeoNet, the European Network of Excellence on the geological storage of $CO_2$ (ENOS newsletter may, 2017). The ENOS project is coordinated by BRGM (France) and unites 19 partners, one of which, CO2GeoNet, comprises 10 of its members as third parties (ENOS newsletter may, 2017). The ENOS partnership strives to advance the development of $CO_2$ storage onshore by investigating whether onshore $CO_2$ storage (CCS) is a safe and viable option to help increase the confidence of stakeholders and the public in CCS as a viable mitigation option to increasing greenhouse gasses (ENOS newsletter may, 2017).

This study contributes to a part of the ENOS project's area of research, where the scope of this study is to investigate the clumped signature on a captured sample of naturally leaking $CO_2$ originating from subsurface sources. The goal is to determine the depth of the $CO_2$ source that vents at the surface.

To date, the majority of previous research on $CO_2$ clumped isotopic species has focused on carbonate clumped isotope thermometry, in which acid digestion of a carbonate mineral yields $CO_2$ having a D47 value dependent on the carbonate crystallisation temperature (Ghosh et al., 2006; Schauble et al., 2006; Guo et al., 2009). It has been used to determine the paleotemperature at the moment of deposition in Carbonate rocks. 'Clumped' isotope geochemistry is the study of multiply substituted isotopologues of naturally occurring molecules, and to date has been used primarily for analysis of mass 47 AMU $CO_2$ (predominantly 13C18O16O) (Dennis et al., 2011). Analyses of the D47 value of atmospheric $CO_2$ have also been used to discriminate among contributions from combustion, respiration, and (in the stratosphere) photochemical reactions (Affek and Eiler, 2006; Affek et al.,2007; Yeung et al., 2009; Hofmann et al., 2017).
This research, focusses on the analyses of D47 of $CO_2$ from naturally leaking subsurface sources with the aim to determine the temperature at the source of $CO_2$-leakage. By applying the geothermal gradient to the temperature indicated by D47 isotopic signatures, it is theorised to provide a range in depth of the $CO_2$ source. The upwards migration $CO_2$ flux, groundwater geochemistry and thermal subsurface conditions play a crucial part in this investigation, and will be investigated for its influence on the δ47 isotopic signals of $CO_2$.

Analysing the clumped signature of venting $CO_2$ is done by cryogenic and chromatographic purification of the collected sample, in order to measure their respective $\delta^{13}C$, $\delta^{18}O$ and Δ47 values on a Thermo-Finnitech MAT 253 mass spectrometer (hereafter IRMS, short for Isotope Ratio Mass Spectrometer), which are used to calculate the depth of the $CO_2$ source. This method is investigated for its feasibility in the use of monitoring $CO_2$ storage sites for subsurface leakage from their storage reservoir and determine whether this originates from the subsurface stored $CO_2$ or another possible source (figure 0).

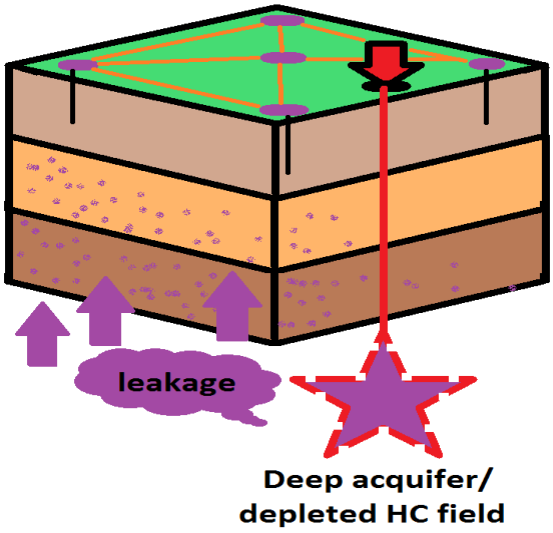


*Figure 0: A schematic overview of a CCS monitoring application. At the red arrow, the $CO_2$ is stored in the subsurface reservoir (Purple star). When the storage location is leaking $CO_2$, it migrates towards the surface, to be detected by a change in local Δ47 geochemistry of venting $CO_2$.*

Figure 1 shows a generalized version of the workflow followed for acquiring and processing the gas samples. In this study, emphasis is put on the analyses of the method in use to determine the d47 clumped isotopic signal from the sampled $CO_2$. Two different methods have been used to evaluate the clumped signal from the sampled gasses, both use the cryogenic purification as the main method of purifying the sampled gasses.

## 3.Method:

### 3.1 Sample acquisition

The sampling campaign was carried out between 27-04-2017 & 31-04-2017 involving a delegation of two partners participating in the ENOS project, University of Rome & TNO. In total four different sampling sites were visited in central Italy; Latera (1), San Vittorino (2), Ailano (3) & Fiumicino (4). The site locations have schematically been indicated in Figure 2.


*Figure 2: A geographic overview of sampling sites in central Italy: Latera (1), San Vittorino (2), Ailano (3) & Fiumicino (4).*

*Figure 1 (below): Generalised workflow overview.*

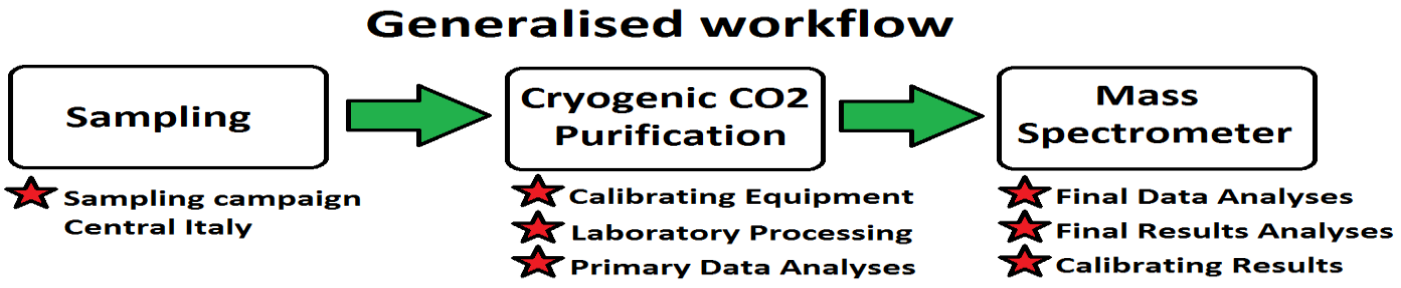

**3.2 Geological setting:**

The study locations of Latera (1), San Vittorino (2), Ailano (3) and Fiumicino (4) all share the common characteristic of $CO_2$ venting at the boundary of the surface and atmosphere, but vary in other characteristics.

Latera is part of the Tuscan Roman Degassing Structure (TRDS) and Campanian Degassing Structure (CDS) (Chiodini et al., 2007). The Latera study site contains a caldera which hosts one of the already discovered high-enthalpy geothermal systems of central Italy (Chiodini et al., 2007) and its subsurface geology has been studied in detail thanks to the Energy National Agency (ENEL) & the joint venture ENEL-AGIP (Barberi et al., 1984 & Bertrami et al., 1984), whom drilled several geothermal wells near Latera. At Latera, the subsurface volcanic formations overlay a complex sedimentary sequence constituted by an allochtonous flysch (Ligurid unit), tectonically emplaced over a carbonate sequence (Tuscan series) (Chiodini et al.,2007). The Flysch deposits form the Caprock of the geothermal system whilst the deeper carbonates form the geothermal aquifers, being recharged via meteoric precipitation on Carbonate outcrops to the North and West of Latera (Chiodini et al., 2007). The reservoir fluid is a CO2-rich water at T of 200 – 300°C and PCO2 of 100 – 200 bars (Chiodini et al., 2007). This temperature range of 200 – 300°C is expected to be indicated measurements on D47 clumped isotopic signature analyses of the sampled CO2, and should indicate a clumped signal of 0.2-0.4‰ (After corrections, and using Wang et al.'s (2004) D47-temperature relation) Analyses performed on the venting gases shows that CO2 forms the largest component of Latera's venting gases (98%) followed by N2, H2S, CH4, Ar, H2, He, and CO (Chiodini et al., 2007). Such a high CO2 composition is a common feature of the TRDS venting gases (Chiodini et al., 2007). At Latera, there are multiple interpretations on the origin of the CO2 where Chiodini et al. (2007) state that the CO2 flux is almost entirely fed by the deep source (98%). Specifically, the geochemistry indicates that CO2 is likely partly produced by thermal metamorphic decarbonation reactions of the Carbonate Aquifers, but it has also a relevant deep component of probable mantle origin, as in the other diffuse degassing structures of central Italy (Chiodini et al., 2004a).

The San Vittorino study location (2) is situated on a plain that is a triangular-shaped intermontane basin filled with fluvial-lacustrine sediments and local travertine deposits, and is surrounded by mountains formed by carbonate and siliciclastic successions thrusted onto various bedrock lithologies (Centamore & Nisio, 2003). The San Vittorino study area is locally characterised by the presence of a large quantity of sinkholes which are formed as the result of chemical reactions of upwards migrating acidic gases (H2S & CO2) along fault locations, interacting with local spring- and ground-waters and the local stratigraphy (Lombardi et al., 2006). The local structural framework greatly influences the CO2 flux towards the surface level. Faulting creates zones of higher permeability and porosity where the CO2 can migrate towards the surface at higher rates near the fault locations (Giustini et al., 2013). While most of the CO2 is attributed to thermal decarbonation of limestone, mantle-derived CO2 is also detected (Giustini et al., 2013). On the local scale, the spatial distribution of the gas vent and of the mantle CO2 contribution suggests that the structural settings in the area strongly control the upward migration of deep fluids (Giustini et al., 2013). The expected temperature ranges and hence Δ47 values for the venting CO2 are unknown at this location.

The Ailano study location (3) has an unknown source of $CO_2$ venting at the surface – atmospheric boundary. It is not known what to expect for the d47 measurements on the acquired samples.

The Fiumicino study location (4) is located in the deltaic alluvial plain, at the mouth of the Tiber River, along the central Tyrrhenian Sea margin, about 30 km from the ultrapotassic volcanic districts of Alban Hills and Mts. Sabatini (Ciotoli et al., 2003). The presence of geothermal gas in the Tiber delta is unusual, based on the site geology. In fact, a variably thick, 40 to 80 m, impermeable cover of clayey to sandy clayey, water saturated, Holocene sediments (*Belluomini et al*., 1986) overlies the several hundred meters thick package of over consolidated, Plio-Pleistocene marine clay deposits, which, in turn, overlies the Meso-Cenozoic carbonate substrate (Mariucci et al., 2008).The CO2 venting at the surface has a deep source of origin (either originated in the mantle or carbonate thermometamorphism) and reaches the surface along faults and fractures in the Quaternary volcanic and sedimentary cover (Ciotoli et al., 2003). The $CO_2$ venting at the surface has a deep source of origin (either originated in the mantle or carbonate thermometamorphism) and reaches the surface along faults and fractures in the Quaternary volcanic and sedimentary cover (Ciotoli et al., 2003). Because of the thick stratigraphy, with thick zones of low permeability,

it is expected that the δ47 clumped signal measured for the captured samples at this site will reflect a lower temperature than its deep source of origin. The expected Δ47 values are hypothesised to reflect the local shallow groundwater temperature.

Whether $CO_2$'s δ47 clumped signal can be used to derive the depth of the subsurface source of origin, depends on the upwards $CO_2$ migration flux vs. the chemical equilibration reactions speed. This will be more elaborately discussed in the Formulae chapter of this report.

When determining whether the δ47 isotopologues of CO2 can be used to infer the depth of the source of origin in the subsurface, the factors of influence and differences between the study sites must be determined and analysed. The factors of influence are divided into four different categories: (1) geological, (2) hydrodynamic, Physical (3), Thermal (4) and (5) chemical. The contributing geological factors can further be divided into: (1.1) structural tectonics, (1.2) stratigraphic-deposits, (1.3) Igneous-deposits with their rock properties and characteristics. The contributing physical factors are further divided into: (3.1) temperature, (3.2) Pressure & (3.3) time. The contributing chemical factors are divided in: (4.1) dissolution reactions of CO2, (4.2) equilibration reactions of CO2 with H2O, (4.3) upwards migration flux, (4.5). The influence and variation of the factors mentioned above on the applicability of using δ47 isotopologues of CO2 to determine its source of origin in the subsurface, can best be modelled in a separate continuation of this study with a numerical modelling based approach. This influence of these characteristics will not be further elaborated upon in this report. A short literary study will be performed on the site locations instead.

These sampling sites have naturally occurring $CO_2$ leakage from a subsurface source, as discussed in the analyses of the geologic setting per sampling site, making them excellent sampling target locations for research in clumped isotopic ratios of $CO_2$. The sampling set-up consisted of a custom made 1L glass Flask, a 6V battery powered vacuum pump, silicone & stainless-steel tubing, a plastic 1L gas sampling bag, a quartz glass tube filled with quartz wool and a drying agent (magnesium perchlorate), a hand vacuum-pump & several different sized funnels. The setup is shown in figure 3 with a schematic representation of the setup shown in figure 4.

*Figure 3: Photograph of gas sampling set-up.*

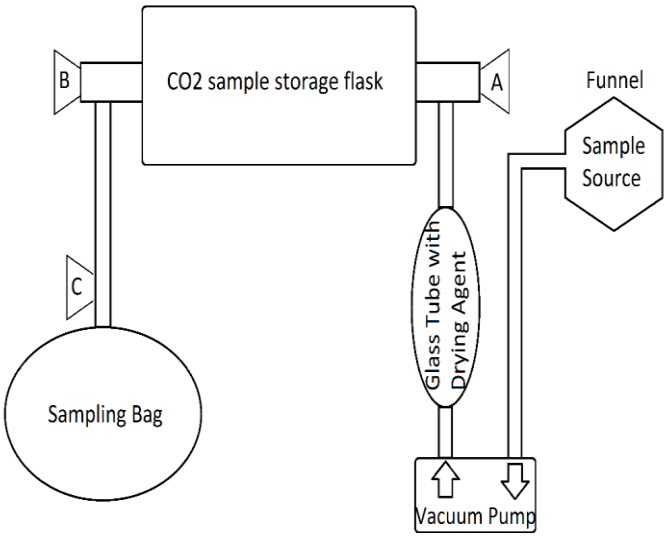


*Figure 4: Schematic of sampling set-up & workflow.*

### 3.3 Sample acquisition workflow

To minimize contamination and resetting of clumped isotopic signatures, the following sample acquisition workflow was systematically exercised. A distinction was made between sampling in "wet" conditions, and sampling in "dry" conditions. Wet sample acquisition occurs where the venting $CO_2$ from a subsurface source venting through surface waters and dry sample acquisition occurs when sampling venting $CO_2$ directly from the soil without water interference.

1. Identify leakage type (wet/dry) and source in field.
2. Set up flask, drying tube, sample bag & vacuum pump by connecting them in a leak tight chain
3. Create a low vacuum with the hand vacuum-pump within the linked system.
4. Place funnel on leakage source with tube attached
5. Attach funnel tube to vacuum pump

6. Open valve A, B & C (figure 4)
7. Turn on vacuum pump
8. Let the 1L sampling bag fill up with the sample gas
9. Empty the sampling bag and repeat step 7
10. Close off valve C (sampling bag) & close valve B (flask)
11. Let vacuum pump build up a small overpressure in flask
12. Close valve A (flask) & turn off vacuum pump
13. Extract two 100 mL volumes from full sampling bag and store in stainless steel canisters
14. Detach Funnel and pack up equipment.

This workflow has been followed when sampling dry and sampling wet, where the only difference in acquisition method is the size of the funnel attached to the vacuum pump. When sampling dry, the outside of the funnel is covered with plastic tarp whilst a fair amount of sand would be deposited on top to minimalize atmospheric contamination (**figure 5**).

*Figure 5: Sampling setup for dry sources.*

As for sampling wet, a larger funnel was used attached with clamps to a wooden beam (Figure 6). This funnel was placed in the water on top of the leakage source and was flushed with the leaking gas prior to sampling. During the sampling, careful attention was paid to keeping the funnel in place over the source and keeping the edge of the funnel slightly below the water surface level to prevent atmospheric contamination. The drying tube is also of importance here for moisture removal, since the influence of water greatly effects the clumped signature of $CO_2$ we intent to measure.

*Figure 6: Sampling set-up for wet sources.*

When sampling at a location is finished, the flask containing the air samples are stored and labelled after the names of the sites visited. All GPS coordinates from the sampling sites have been saved and are displayed in table 1. A total of 10 samples were acquired for isotope analyses.

| Sample label | Sampling Date | Location | Latitude | Longitude |
|---|---|---|---|---|
| Latera I | 29-04-2017 | Latera | 42°37'4.70"N | 11°49'6.59"O |
| Latera II | 29-04-2017 | Latera | 42°36'6.37"N | 11°48'57.77"O |
| Latera III | 29-04-2017 | Latera | 42°35'10.07"N | 11°47'24.77"O |
| San Vittorino 6A | 29-04-2017 | San Vittorino | 42°22'28.59"N | 12°59'47.77"O |
| San Vittorino 6B | 29-04-2017 | San Vittorino | 42°22'28.46"N | 12°59'47.73"O |
| San Vittorino 18 | 29-04-2017 | San Vittorino | 42°22'13.62"N | 12°59'16.77"O |
| Ailano I | 30-04-2017 | Ailano | 41°22'59.48"N | 14°11'45.25"O |
| Ailano II | 30-04-2017 | Ailano | 41°23'1.48"N | 14°11'48.92"O |
| Ailano IIIA | 30-04-2017 | Ailano | 41°23'4.18"N | 14°10'41.04"O |
| Ailano IIIB | 30-04-2017 | Ailano | 41°23'4.18"N | 14°10'41.04"O |
| Fiumicino I | 30-04-2017 | Fiumicino | 41°45'41.16"N | 12°16'46.79"O |

*Table 1: Overview of samples, locations and coordinates*.

The sampled gas composition has been measured by the University of Rome and is displayed in the table below (Table 2). Since the Table 2's values are necessary inputs for the cryogenic processing methods used in this research, it is necessary to discuss them at this point in the report. The sulfuric gas components are missing from the table below because they are

| Sample | Cannister | [PPM] He | % CH4 | [PPM] C2H6 | [PPM] C3H8 | % $CO_2$ | % O2+Ar | % N2 | % Total |
|---|---|---|---|---|---|---|---|---|---|
| Latera I | 1 | 7,44 | 0,09 | 8,90 | 1,20 | **94,15** | 1,03 | 4,66 | **99,93** |
| | 2 | 7,37 | 0,09 | 8,90 | 1,20 | **98,00** | 0,68 | 3,58 | **102,35** |
| Latera II | 1 | 0,09 | 0,01 | 0,98 | | **96,00** | 1,06 | 3,88 | **100,95** |
| | 2 | 0,19 | 0,01 | 1,20 | | **96,00** | 1,30 | 4,62 | **101,93** |
| Latera III | 1 | 5,86 | 0,10 | 10,00 | 1,70 | **97,00** | 0,74 | 2,96 | **100,80** |
| | 2 | 5,77 | 0,10 | 9,80 | 1,85 | **94,35** | 0,85 | 3,28 | **98,58** |
| San Vittorino 6A | 1 | 40,27 | 0,05 | 6,60 | | **80,00** | 2,78 | 15,32 | **98,15** |
| | 2 | 33,74 | 0,06 | 6,60 | | **81,00** | 2,50 | 14,50 | **98,06** |
| San Vittorino 6B | 1 | 23,49 | 0,05 | 6,00 | | **87,50** | 2,03 | 12,15 | **101,73** |
| | 2 | 30,20 | 0,05 | 6,40 | | **86,10** | 1,74 | 10,98 | **98,87** |
| San Vittorino 18 | 1 | 17,11 | 0,02 | 0,80 | | **88,25** | 2,06 | 9,60 | **99,93** |
| | 2 | 19,98 | 0,02 | 0,75 | 0,03 | **88,50** | 2,44 | 10,68 | **101,64** |
| Ailano I | 1 | 6,24 | 0,36 | 2,60 | 0,70 | **94,00** | 1,40 | 6,60 | **102,36** |
| | 2 | 6,05 | 0,35 | 2,80 | 0,90 | **93,50** | 1,31 | 6,24 | **101,40** |
| Ailano II | 1 | 6,15 | 0,36 | 2,40 | 0,70 | **88,75** | 1,63 | 7,42 | **98,16** |
| | 2 | 0,17 | 0,20 | 2,80 | 1,18 | **91,00** | 1,72 | 6,52 | **99,44** |
| Ailano IIIA | 1 | 0,38 | 0,21 | 3,50 | 1,13 | **91,00** | 2,06 | 8,12 | **101,39** |
| | 2 | 0,99 | 0,22 | 2,00 | 0,79 | **95,00** | 1,62 | 6,32 | **103,16** |
| Ailano IIIB | 1 | 1,04 | 0,22 | 2,20 | 0,75 | **93,00** | 1,64 | 6,42 | **101,28** |
| | 2 | 0,95 | 0,22 | 2,20 | 0,78 | **94,50** | 1,34 | 5,42 | **101,48** |
| Fiumicino I | 1 | 5,02 | 0,00 | 0,08 | | **20,60** | 15,96 | 61,66 | **98,22** |
| | 2 | 4,99 | 0,00 | 0,06 | | **22,50** | 15,30 | 59,00 | **96,80** |

*Table 2: An overview of the sample gas composition. After S.E. Bienbeau., University of Rome.*

below detection limit. They are however present in some? of the samples, which has been determined by a rotten egg smell that is being released whilst processing the sample in the $CO_2$ purification set-up.

As can be observed from the table above (Table 2), the concentration of $CO_2$ contained within the sample flasks range from 22,5% - 98,0%, with the majority of the sample $CO_2$ concentrations near the high end of this range.

### 3.4 $CO_2$ purification

A diluted version of the originally sampled gasses has been made using a vacuum line, a gastight syringe and gaseous nitrogen as the dilution agent. The diluted samples serve as a secondary method to process the air samples acquired. An overview of these diluted samples is given in Table 3. With the gastight syringe, some of the sample gas is extracted from the sample flask, and diluted with 1000 mL of gaseous nitrogen in a new flask labelled: sample + dil., after the original sample.

### 3.5 Method 1: IRMS connected cryogenic CO2 Purification

mL $CO_2$ injected into MS:

$CO_2$***_injected(mL) =***

***Freezetime (s) * (Flowrate/60) (mL/s) * [$CO_2$] Sample (%)***

(0)

Using the CO2 concentration data per sample shown in Table 2, it is calculated how much $CO_2$ is introduced into the purification-set-up using formula 0, in order to output 1.33 mL of pure $CO_2$ into the IRMS. This is done by varying the two input variables: Freezetime (s) & Flowrate (mL/s) related to a fixed concentration value specific to the to measure sample (table 2). Freezetime indicates the time in seconds where the introduced sampled air is cooled by liquid nitrogen at =-194*C. Flowrate is the rate at which a fixed quantity of sample gas is introduced per time unit using a mass flow controller unit (mL/s). Table 4 displays values solved

| Diluted Samples | Sample $CO_2$ [PPM] | Sample $CO_2$ [%] | Sample extracted (mL) | $CO_2$ (mL) | N2 added (mL) | Total Volume (mL) | Diluted Sample [PPM] | Diluted Sample [%] | Dilution Factor |
|---|---|---|---|---|---|---|---|---|---|
| **S.Vitt 6a dil.** | 800000 | 80 | 4 | 3,2 | 1000 | 1004 | 3187 | 0,32 | 251 |
| **Fiumicino dil.** | 210000 | 21 | 10 | 2,1 | 1000 | 1010 | 2079 | 0,21 | 101 |
| **S.Vitt 6b dil.** | 870000 | 87 | 4 | 3,48 | 1000 | 1004 | 3466 | 0,35 | 251 |
| **S.Vitt 18 dil.** | 860000 | 86 | 4 | 3,44 | 1000 | 1004 | 3426 | 0,34 | 251 |
| **Ailano 1 dil.** | 920000 | 92 | 4 | 3,68 | 1000 | 1004 | 3665 | 0,37 | 251 |
| **Ailano 2 dil.** | 910000 | 91 | 4 | 3,64 | 1000 | 1004 | 3625 | 0,36 | 251 |
| **Ailano 3a dil.** | 930000 | 93 | 4 | 3,72 | 1000 | 1004 | 3705 | 0,37 | 251 |
| **Ailano 3b dil. (doublet)** | 940000 | 94 | 4 | 3,76 | 1000 | 1004 | 3745 | 0,37 | 251 |
| **Latera 1 dil.** | 960000 | 96 | 4 | 3,84 | 1000 | 1004 | 3825 | 0,38 | 251 |
| **Latera 2 dil.** | 960000 | 96 | 4 | 3,84 | 1000 | 1004 | 3825 | 0,38 | 251 |
| **Latera 3 dil.** | 950000 | 95 | 4 | 3,8 | 1000 | 1004 | 3785 | 0,38 | 251 |

*Table 3: Diluting $CO_2$ Samples to lower concentrations.*

using formula X for 1.33 mL $CO_2$ injected into the mass spectrometer with a constant set flowrate of 15 mL/min for samples, 50 ml/min for diluted samples and 100 ml/min for reference gasses (0.25 mL/s, 0.83 mL/s & 1.67 mL/s respectively). The wait1 & wait2 variables are constants determined prior to measurement, related to the thawing and freezing of $CO_2$ within the cryogenic purification set-up, and will not be varied during the performed measurements.

Besides the measuring samples, two reference gasses have also routinely been measured in between the sample measurement cycles in order to determine whether the $CO_2$ purification set-up and IRMS are performing consistent and accurate measurements.

The accuracy of the $CO_2$ purification set-up was first calibrated by purifying two types of reference gasses, and measuring the pure $CO_2$ on the mass-spectrometer for its clumped d47 signature. The reference gasses stem from the same "Scott's $CO_2$ cylinder" which is mixed with synthetic air to a concentration in ppm closely resembling atmospheric concentrations. In one cylinder, the Scott's air mix has been heated to 1000°C in quartz glass tube housed in a furnace and kept at this 1000*C for four hours. After the four hours have passed, the heated quartz tube is taken out of the furnace and rapidly cooled in a water bath to room temperature. This process ensures that the clumped CO2 signature for 1000*C is maintained. The heated Scott's air mix is injected in a vacuum line and frozen in a trap cooled by liquid nitrogen. The frozen $CO_2$ is slowly released in an empty gas cylinder, after which, synthetic air has been added to dilute the $CO_2$ housed within the cylinder. The cylinder afterwards is measured to determine the final concentration of $CO_2$ within, totalling 438 ppm of $CO_2$ with a heated clumped signature. This heated clumped signature standard has been labelled Scott's Heated XI. The second gas cylinder is also prepared with the Scott's air mix. However, for the second cylinder the $CO_2$ has not been heated, and resembles the clumped isotopic values for $CO_2$ equilibrated at room temperature (25°C) CO2. The

| **Samples** | $CO_2$ **[%]** | **Flowrate (mL/s)** | **Freezetime (s)** | **Wait1 (s)** | **Wait2 (s)** | $CO_2$**_injected (mL)** |
|---|---|---|---|---|---|---|
| Latera I | 96 | 0.25 | 5.54 | 1800 | 2000 | 1.33 |
| Latera II | 96 | 0.25 | 5.54 | 1800 | 2000 | 1.33 |
| Latera III | 96 | 0.25 | 5.54 | 1800 | 2000 | 1.33 |
| San Vittorino 6A | 80 | 0.25 | 6.65 | 1800 | 2000 | 1.33 |
| San Vittorino 6B | 86 | 0.25 | 6.19 | 1800 | 2000 | 1.33 |
| San Vittorino 18 | 87 | 0.25 | 6.10 | 1800 | 2000 | 1.33 |
| Ailano I | 94 | 0.25 | 5.67 | 1800 | 2000 | 1.33 |
| Ailano II | 90 | 0.25 | 5.91 | 1800 | 2000 | 1.33 |
| Ailano IIIA | 93 | 0.25 | 5.72 | 1800 | 2000 | 1.33 |
| Ailano IIIB | 94 | 0.25 | 5.66 | 1800 | 2000 | 1.33 |
| Fiumicino I | 21 | 0.25 | 26,6 | 1800 | 2000 | 1.33 |
| | | | | | | |
| **Diluted Samples** | | | | | | |
| Latera I dil. | 0.38 | 0.83 | 422 | 1800 | 2000 | 1.33 |
| Latera II dil. | 0.38 | 0.83 | 422 | 1800 | 2000 | 1.33 |
| Latera III dil. | 0.38 | 0.83 | 422 | 1800 | 2000 | 1.33 |
| San Vittorino 6A dil. | 0.32 | 0.83 | 501 | 1800 | 2000 | 1.33 |
| San Vittorino 6B dil. | 0.35 | 0.83 | 458 | 1800 | 2000 | 1.33 |
| San Vittorino 18 dil. | 0.34 | 0.83 | 471 | 1800 | 2000 | 1.33 |
| Ailano I dil. | 0.37 | 0.83 | 433 | 1800 | 2000 | 1.33 |
| Ailano II dil. | 0.36 | 0.83 | 445 | 1800 | 2000 | 1.33 |
| Ailano IIIA dil. | 0.37 | 0.83 | 433 | 1800 | 2000 | 1.33 |
| Ailano IIIB dil. | 0.37 | 0.83 | 433 | 1800 | 2000 | 1.33 |
| Fiumicino I dil. | 0.21 | 0.83 | 763 | 1800 | 2000 | 1.33 |
| | | | | | | |
| **Reference Gas (standards)** | | | | | | |
| Scott's Unheated | 0.04 | 1.67 | 2000 | 1800 | 2000 | 1.33 |
| Scott's Heated X | 0.04 | 1.67 | 2000 | 1800 | 2000 | 1.33 |
| Scott's Heated XI | 0.04 | 1.67 | 2000 | 1800 | 2000 | 1.33 |

*Table 4: Summary of cryogenic $CO_2$ Purification processing input variables.*

cylinder is filled in a similar manor, with the final concentration of $CO_2$ determined at 400 ppm. The unheated clumped signature standard has been labelled Scott's Unheated.

These two reference gasses thus contain two types of clumped isotopic signatures, representing two calibration points for clumped signatures linked to a fixed temperature. A second cylinder containing the Scott's unheated CO2 is attached to the reference bellow of IRMS. Consistently and routinely measuring these standards on the mass spectrometer is crucial for two reasons. First of all, by measuring the purified $CO_2$ from the unheated gas cylinder against the unprocessed CO2 from the Scott's air cylinder, it can be quantified how much the cryogenic $CO_2$ purification method effects the clumped isotope signal for $CO_2$. An offset measured between the unprocessed $CO_2$ vs. the processed purified $CO_2$ occurs due to the process of isotopic fractionation inside the cryogenic $CO_2$ set-up. Fragmentation and recombination reactions are plausibly responsible for variations on the order of 10%, relative, in measured D47 values of $CO_2$ gases (Affek et al., 2009; Huntington et al., 2009; Passey et al., 2010). The final results have to be corrected for this effect.

Secondly, the measured clumped isotopic signatures obtained for the two reference gasses with a known temperature is used to calibrate the clumped isotopic signature measured for $CO_2$ from the processed samples to a temperature fitting curve. An empirical transfer function is used to convert data to a common absolute reference frame that is based on the theoretical temperature dependence of equilibrium clumping in $CO_2$ (Wang et al., 2004). If D47 values are to be measured consistently and with absolute

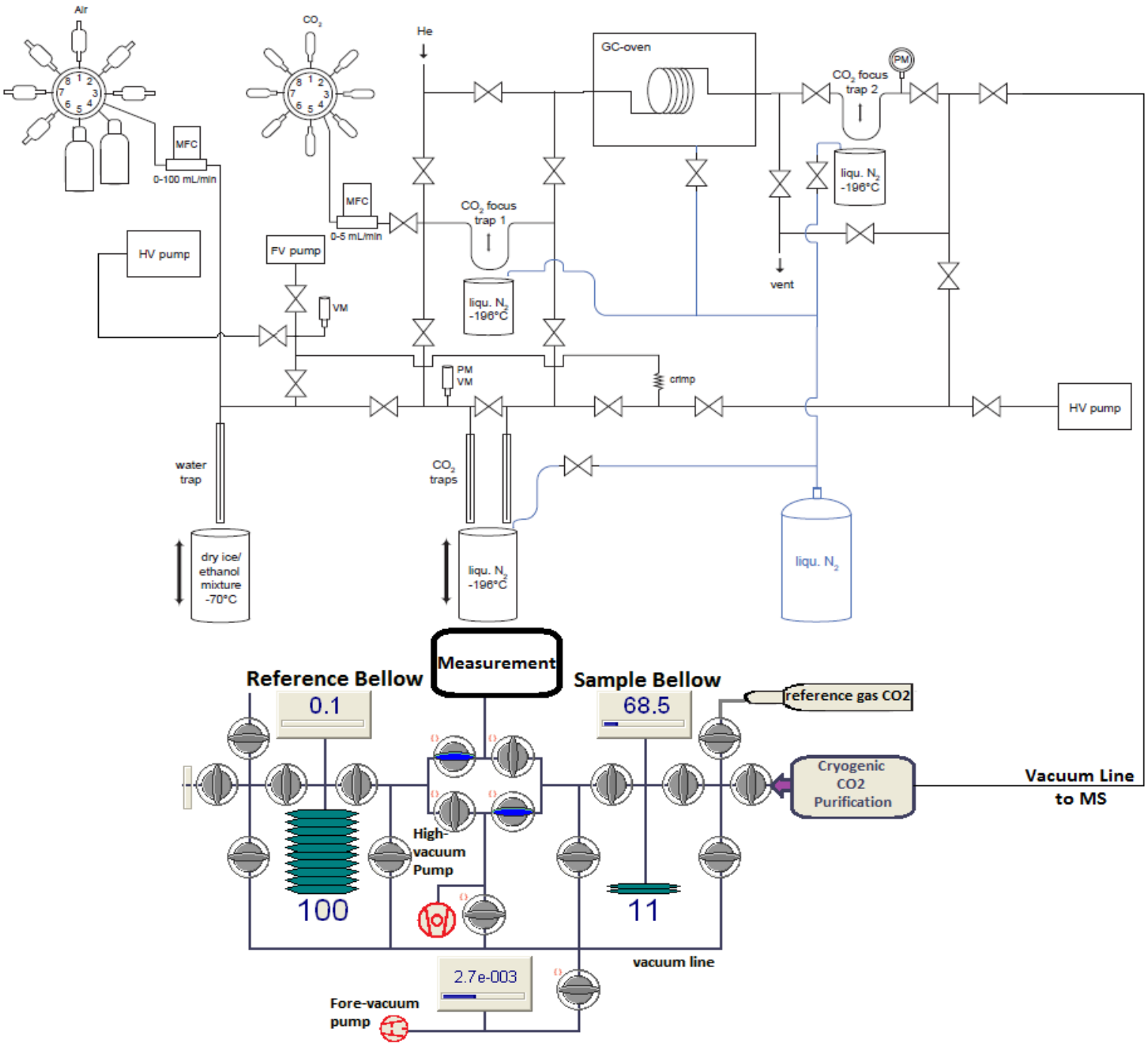


*Figure 7: Cryogenic $CO_2$Purification processing set-up created by M.E.G. Hofmann (2017)*

accuracy as good as the external precisions of the best measurements (0.005–0.010‰), we must directly account for these source 'scrambling' effects (Dennis et al., 2011). Adding to these source scrambling corrections, we also correct for the presence of $N_2O$ on mass 47 and correct for the amount of isotopic fractionation occurring when cryogenically purifying $CO_2$ from other gasses contained within the samples. These corrections will be explored later in this report.

**Figure 7** displays the cryogenic $CO_2$ purification set-up created by M.E.G. Hofmann (Hofmann et al., 2017), which has been created to measure clumped isotopic signatures of atmospheric $CO_2$. The accuracy of the set-up has been determined to be in the range of 0.04‰ (Hofmann et al., 2017). This is more lenient compared to the proposed 0.005–0.010‰ by Dennis et al. (2017). The cryogenic purification set-up is attached to mass spectrometer inlet.

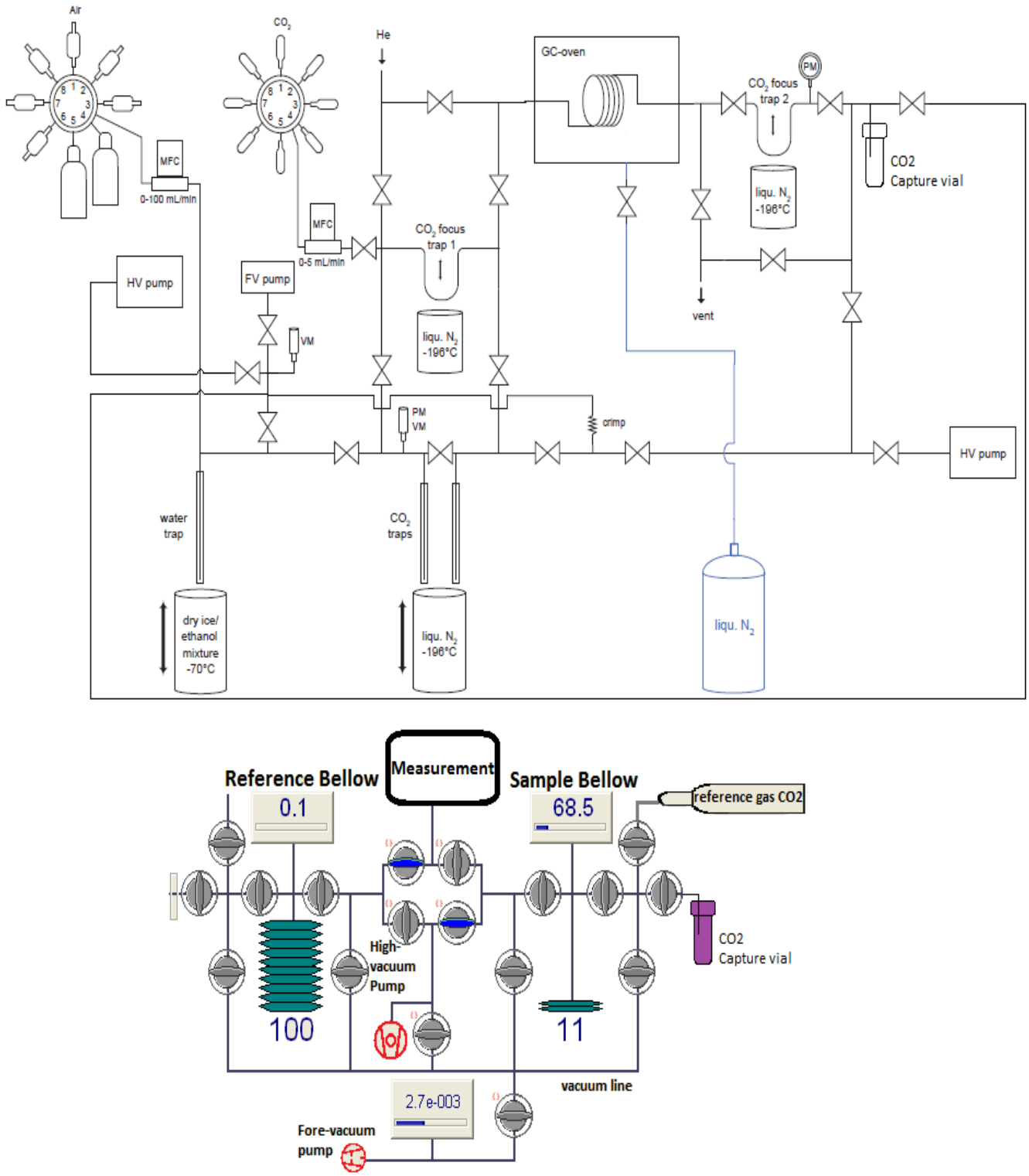


*Figure 8: Method 2: Adaptations made to the cryogenic purification process by BM (Appendix 1).*

### 3.6 Method 2: cryogenic $CO_2$ purification of samples

An adaptation on the on-line cryogenic $CO_2$ purification was undertaken to be able to purify the samples off-line (**Figure 8**). The most significant changes made to the $CO_2$ purification set-up are; (1) The connection to the mass spectrometer sample bellow inlet was detached and instead a sample capture vial was connected. Furthermore, (2) the liquid nitrogen dewer filling system was removed, to be able to refill the dewers manually and (3) the liquid nitrogen hose was attached to directly the oven which houses the GC column. Finally, (4) a smaller diameter connector replaced the original connection between the oven and the liquid nitrogen tank. There were no significant changes in the workflow posted in Figure 1 & Figure 9. Since there are no measurement results from using method 2, it will be not be discussed in detail, and the

detailed implications of these changes are added to this report as appendix 1.

**3.7 Formulae:**

This section will briefly discuss the formulae relevant to the equilibration of $CO_2$ with subsurface waters and the formulae used in the calculation of Δ47 using an IRMS device.

Δ47 isotopologues of $CO_2$ approaches zero at high temperatures and increases at low temperatures, reflecting a slight thermodynamic preference for two heavy isotopes to bind with each other (Affek (2013)). Δ47 is formally defined through the self-reaction of isotopic exchange amongst the $CO_2$ isotopologues (Eiler & Schauble, (2004); Wang et al., (2004)):

$$^{12}C^{16}O^{16}O + {}^{13}C^{18}O^{16}O \leftrightarrow {}^{13}C^{16}O^{16}O + {}^{12}C^{18}O^{16}O$$

(Reaction 1)

Exchange of $CO_2$ isotopologues is catalysed by chemical reactions with local hydrology, thus linking Δ47 and $\delta^{18}O$ through the set of reactions (Affek (2013):

$$^{12}C^{16}O^{16}O + H_2{}^{18}O \leftrightarrow$$

$$H_2{}^{12}C^{16}O^{16}O^{18}O + {}^{12}C^{18}O^{16}O + H_2{}^{16}O \qquad \text{(Reaction 2)}$$

$$^{13}C^{16}O^{16}O + H_2{}^{18}O \leftrightarrow$$

$$H_2{}^{13}C^{16}O^{16}O^{18}O + {}^{13}C^{18}O^{16}O + H_2{}^{16}O \qquad \text{(Reaction 3)}$$

The rate that Δ47 approaches equilibrium is determined by exchange with water and therefore the time required to reach Δ47 equilibrium is the same as that for $\delta^{18}O$ (Affek (2013)). This research focuses on the investigation of Δ47 clumped signals measured of venting $CO_2$ from a subsurface source. During the sample acquisition campaign ground water samples were taken at the study site locations where the wet sources specific sampling acquisition method was applied (figure 6). These samples have not been analysed for their $\delta^{18}O$ values, but do offer a good control on the accuracy of the Δ47 clumped isotopic signature measured from the venting $CO_2$ from a subsurface source, and processed on the IRMS. However, since the independence of equilibrium Δ47 of the composition of water with which $CO_2$ chemically reacts, implicates that Δ47 is a better indicator for incomplete exchange when compared with $\delta^{18}O$ so that it can be used to identify and potentially quantify the extent of disequilibrium in either gas phase CO2 or in CaCO3 minerals (Affek (2013)). As for the reaction speed, rate constants were calculated by Clog et al. (2015) and were equal for the evolution of δ18O and Δ47 at each temperature (within the margin of error). They averaged at:

$$0.19\ ‰\ h^{-1} \text{ at } 5\ °C,\ 0.38\ ‰\ h^{-1} \text{ at } 25\ °C \text{ and}$$

$$0.65\ ‰\ h^{-1} \text{ at } 37\ °C.$$

These results show an increasing isotopic exchange rate constant for Δ47 isotopologue exchange at increasing temperatures, for low temperature ranges.

Using the mass 47 anomaly parameter (Δ47) defined as the deviation of the isotope ratio $R^{47}$ (=[47]/[44]) from that at a random distribution of isotopes among all isotopologues, Δ47 is calculated as such (Affek (2013)):

Δ47 =

$$[(R^{47}/(2R^{13} * R^{18}+2R^{17} * R^{18}+R^{13} * (R^{17})^2)) - (R^{46} / (2R^{18}+2R^{13} * R^{17}+(R^{17})^2)) - (R^{45} / (R^{13} + 2R^{17}))+1] * 1000 \quad (4)$$

Where $R^{13}$, and $R^{18}$ are obtained by traditional isotopic measurements of masses $R^{45}$ and $R^{46}$ that are measured simultaneously with $R^{47}$ with an IRMS device, and $R^{17}$ is estimated through its mass dependent relationship with $R^{18}$ (Affek & Eiler (2006)). Appendix 2C has a more elaborate display of the Formulae used to calculate the Δ47 values displayed in this research. For the sake of brevity, the formulae concerning $CO_2$'s reactivity with water and the calculation of Δ47 will not be explored further beyond what has already been written.

**Thermo-Finnitech MAT 253 Dual Inlet mass spectrometer**

The isotope measurements are performed on a Thermo-Finnitech mat 253 dual inlet mass spectrometer (IRMS) (Figure 7 & 8), adapted with a $5^{th}$ faraday cup to collect simultaneously mass 47. To date, published measurements have all used a Thermo-Finnitech MAT 253 configured to collect masses 44 through 48 or 49 (Dennis et al., 2011). The mass spectrometer contains two bellows, where one is filled with the to measure purified sample gas, and one is filled with a reference gas, in this case: Scott's $CO_2$ from an attached cylinder. In order to perform an accurate measurement several procedures need to be followed to prepare the mass spectrometer system for measurement.

The reference gas is filled in the reference bellow being stretched out fully (100%) up to a level which reads 13000 mV on m/z 44. It is crucial to refill the sample bellow to these levels for a reliable and accurate

measurement since the mass spectrometer is very sensitive to pressure differences between the bellows. The minimum pressure difference indicated in mV for a successful measurement is 300 mV, any higher registered pressure differences result in anomalous data outputs by the mass spectrometer. The most important process is thus controlling the amount of $CO_2$ injected into the sample bellow of the mass-spectrometer. If less than 1.33 mL is injected into the mass spectrometer it will always result in a failed measurement. If anything more than 1.33 mL is introduced into the reference bellow can automatically adjust to overcome the initial pressure difference. The maximum pressure adaptation is however limited to an unknown maximum amount of sample. After the reference bellow has been filled to the level indicated with the Scott's $CO_2$ reference gas, the mass spectrometer waits for the signal to fill up the sample bellow with sample gas that was processed and transferred by a vacuum pump in the IRMS set-up. By using the $CO_2$ sample concentration (Table 4) as a starting point, it is calculated how much $CO_2$ to input into the cryogenic purification set-up in order to output 1.33mL to the mass spectrometer to be filled in the sample bellow. The measurement of a sample constitutes of eight sequential cycles (n=8) where a sample gas is measured against a reference gas under equal pressures.

## 4.Data Processing

### 4.1 Workflow

In order to determine the clumped isotopic signature of the $CO_2$ samples obtained in Italy, the data processing workflow concerning $CO_2$ isotopologue analyses ((Figure 9) M.E.G. Hofmann (2017)) was implemented. Here the $R^{12}$, $R^{13}$, $R^{16}$, $R^{17}$, $R^{18}$, $R^{44}$, $R^{45}$, $R^{46}$, $R^{47}$, $R^{48}$ & $R^{49}$ are measured along with their corresponding standard deviation & Standard Error. These R-values are used to calculate the Δ47 clumped isotopic signal of CO2. The excel sheet containing the raw data is created in Isodat by reprocessing the raw output data from the mass spectrometer. The program Isodat itself is not used any further than RAW data extraction. This reprocessed raw data is filtered by an excel macro in order to filter out redundant information stored in the original raw file. The filtered Data is then imported into an excel calculation sheet, which houses the formulae to calculate the isotope ratios in delta notations of the sample measured. The final step corrects the initial results for the presence of $N_2O$ and fractionation, since the GC column built in the $CO_2$ purification set-up is not capable of accurately separating $N_2O$ from $CO_2$ and fractionation of isotopologues occurs within the cryogenic set-up. The final results are analysed and compared to the values obtained for the measured reference gas standards, with emphasis put on the difference in m/z=47 representing the clumped signature of $CO_2$ which is fitted to an ETF temperature curve to extrapolate the associated temperature.

There are three important corrections performed on the initial results: fractionation, scramble drift and $N_2O$ presence. The correction calculations have been attached to this report as appendix 3. The correction calculations have been created by M.E.G. Hofmann in her previous work on clumped isotopic analyses. After all measurements have been corrected for $N_2O$

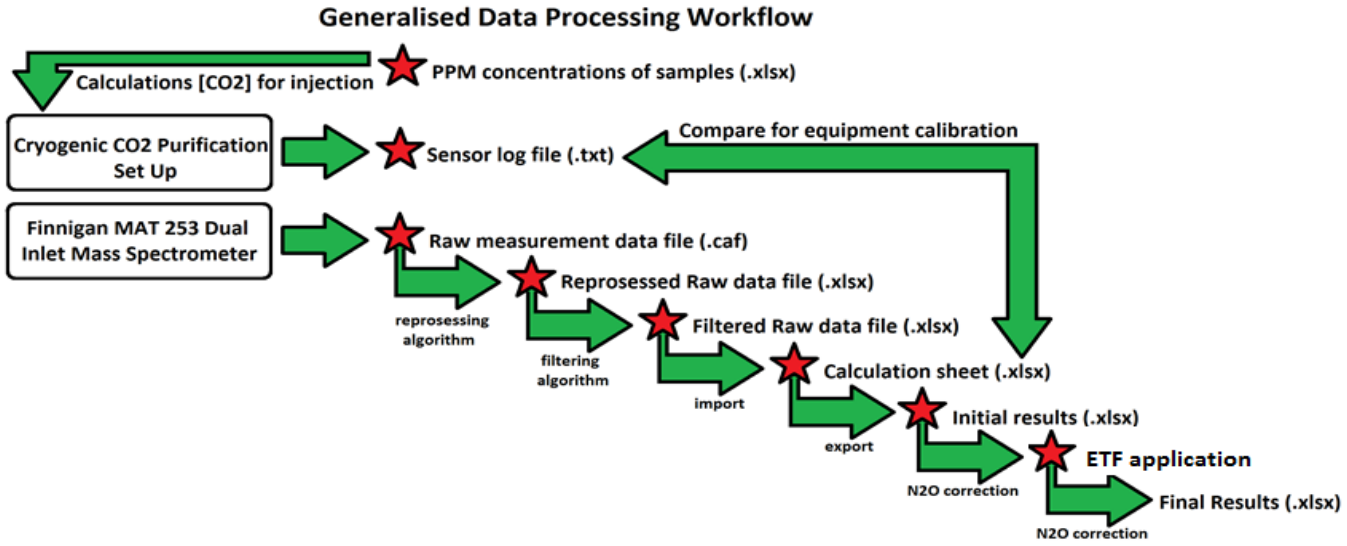


*Figure 9: Generalised data processing workflow overview.*

| REFERENCE GASSES | AVG. D47 | AVG. D47 ST.DEV | AVG. D47 SE | AVG. D13C | AVG. D13C ST.DEV | AVG. D18O | AVG. D18O ST.DEV | T*C [ETF] | N |
|---|---|---|---|---|---|---|---|---|---|
| **SCOTT AIR MIX UNHEATED** | 0,157 | 0,045 | 0,019 | -2,781 | 0,024 | -5,875 | 0,026 | 25 | 4 |
| **SCOTT AIR MIX HEATED** | -0,521 | 0,039 | 0,014 | -2,604 | 0,021 | -6,214 | 0,026 | 1000 | 6 |

*Table 5: Averaged results of all performed measurements on reference gasses using set-up 1.*

contamination the final results are obtained for the D47 values.

**4.1 Assumptions made prior to measurement**

Prior to measurement, several assumptions have been made. (1) The purified samples are clean samples, (2) the isotopic fractionation occurred during processing is correctable, (3) the acquired air samples were sufficiently dry to retain their clumped signature, (4) the influence of isotopic equilibration by water in the cryogenic purification set-up is negligible, (5), and, (6) the sampled $CO_2$ migrating upwards, venting at the surface did not have time to isotopically equilibrate with the ground water, losing its original d47 clumped signal. The validity of these assumption will be tested in the discussion section of this report.

**Measurements Results**

The finalised results are divided in two sections, distinguishing between: (1) initial results & (2) final results. The initial results have not been corrected for fractionation nor $N_2O$ presence, whilst the final results have been corrected for fractionation and $N_2O$ presence. The data has been acquired by following processing method 1 (figure 7): the IRMS connected $CO_2$ processing set-up. Before performing further calculations on the processed data, a summary of the initial raw D47 results are given in Tables 5 & 6 to be analysed and checked.

**4.2 Initial results: reference gases**

The initial results for processed and measured $CO_2$ reference gases are presented in Table 5, where for now the emphasis is put on analyses of the d47 vs. T (°C) relationship. This relationship is obtained from plotting the D47 values from the two $CO_2$ reference gasses with their known temperature correlation as standards using an IRMS. This D47 vs T°C relationship is analysed by first deriving and applying an Empirical Transfer Function (hereafter: ETF). The ETF has be to be constructed from the D47 results of the measured reference gasses (Table 5) before any indication of a temperature can be given for the sample gasses.

**4.3 Empirical Transfer Function**

To Determine the temperature related to the measured d47 values for the processed samples, an absolute reference frame (Dennis et al., 2004) needs to be established first. Via this absolute reference frame an ETF can be derived to extrapolate a temperature vs D47 relationship. This is done by initially comparing the D47 values obtained through IRMS measurements performed for the reference gasses, to the generally accepted values of D47 for $CO_2$ isotopologues

| | D47 Wang et al. (2004) | D47 IRMS measurements | D47 Utrecht University | D47 Yale University | D47 California institute of technology | D47 Harvard University | D47 John Hopkins University |
|---|---|---|---|---|---|---|---|
| 1000*C | 0.0266 | -0,521 | -0.75 | -0.8431 | -0.7869 | -0.9182 | -0.8686 |
| 50*C | 0.8050 | X | X | -0.1094 | -0.0957 | -0.1473 | -0.1002 |
| 27*C | 0.9147 | X | X | X | X | X | -0.0077 |
| 25*C | 0.9252 | 0.157 | 0.20 | 0.0013 | -0.0271 | -0.0216 | X |
| 10*C | 1.0089 | X | X | 0.0812 | X | 0.0480 | X |
| 8*C | 1.0208 | X | X | X | 0.0788 | X | X |
| 0*C | 1.0705 | X | X | X | X | X | 0.1412 |

*Table 6: D47 values overview. X represents an absence of measurement data on D47 vs calibrated $CO_2$ at the known temperature. The Values presented by Wang et al. (2004) are generally accepted values and will be used as a ground truth for D47. This table is after the values presented in Dennis et al. (2011).*

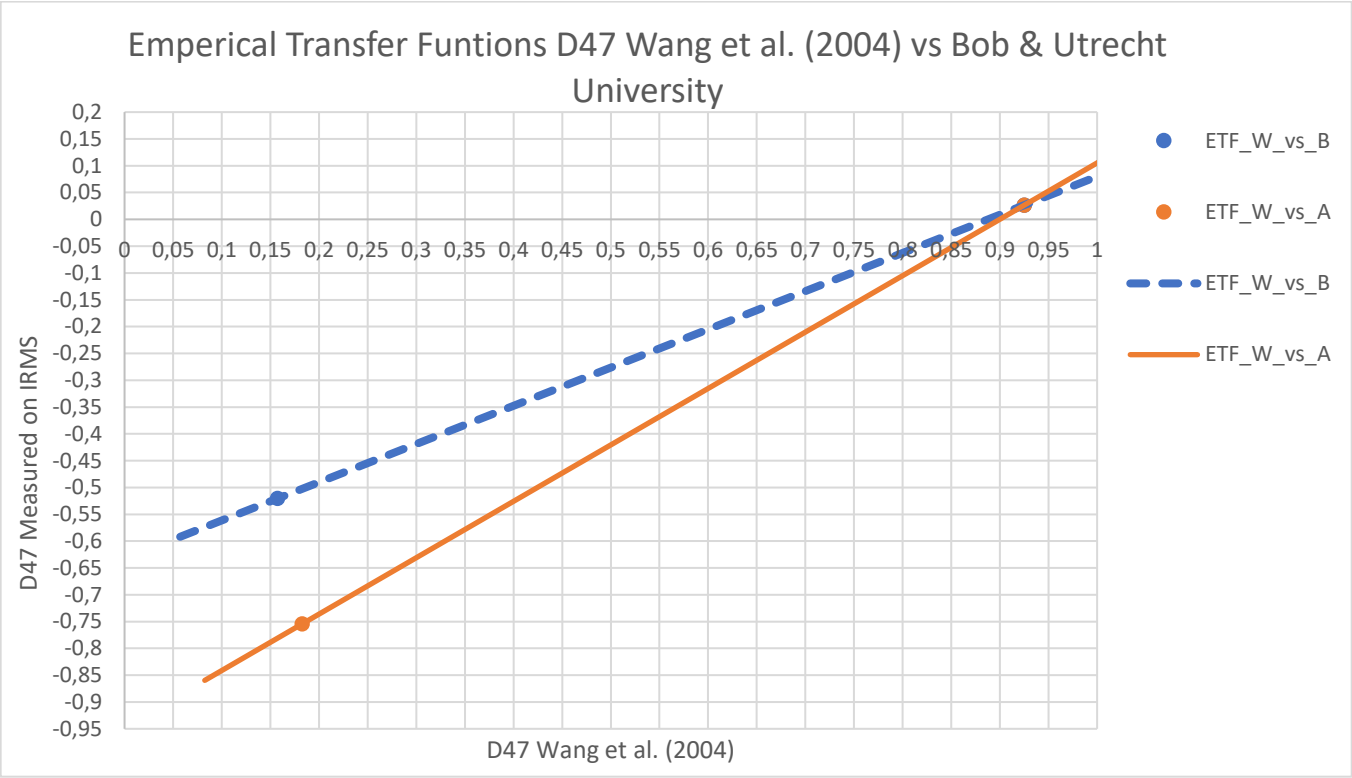


*Graph 1: ETF functions Derived from the measured standards (blue) and derived from measured $CO_2$ gas standards by Utrecht University.*

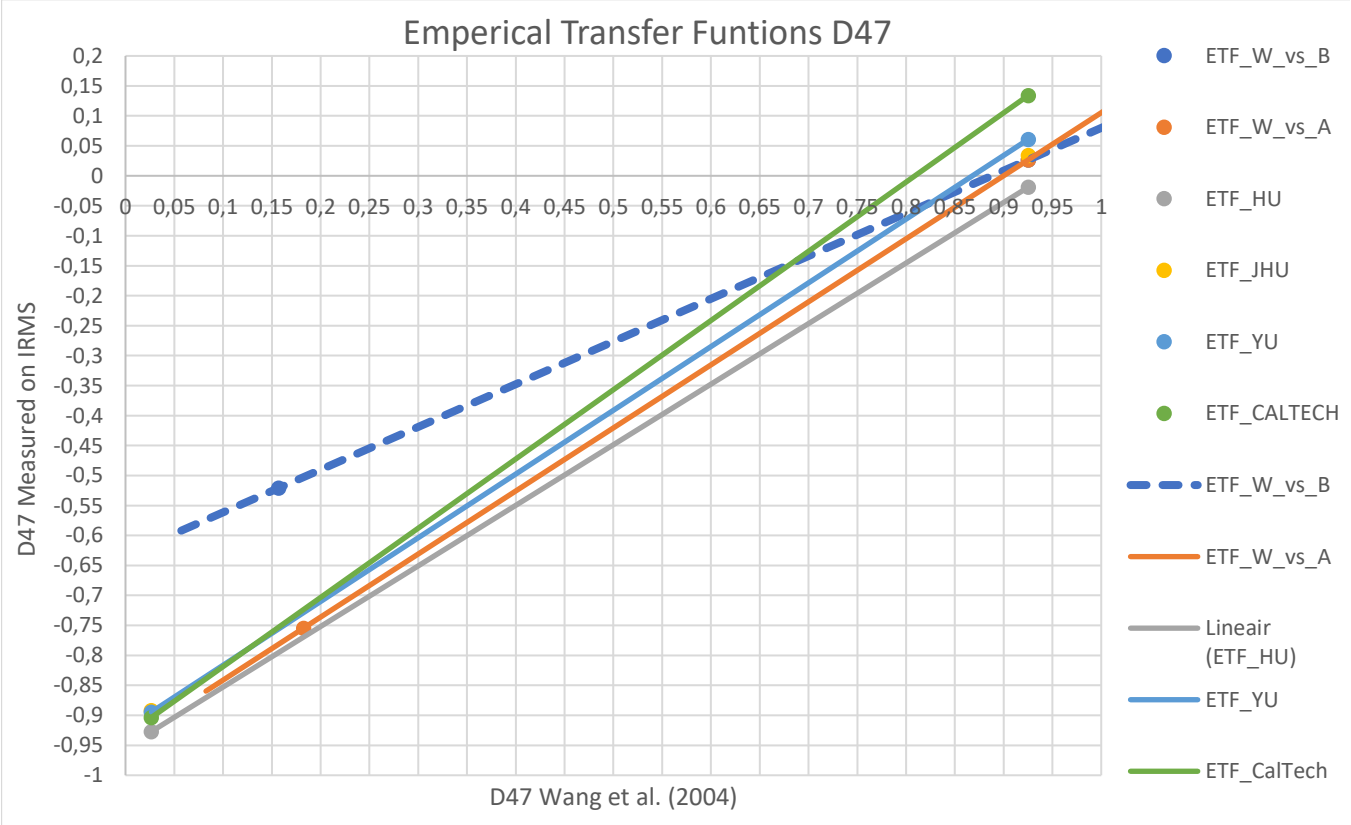


*Graph 2: an overview of several ETF functioned plotted against the D47 values presented by Wang et al. (2004) as an assumed ground truth. Laboratories listed in the legend from Top to bottom: Bob, Utrecht University, Harvard University, John Hopkins University, Yale University and California Institute of Technology. The data for constructing the ETF functions and associated values from all laboratories except for Utrecht University & Bob (this research), have been obtained from Dennis et al. (2011).*

calibrated at specified temperatures presented by

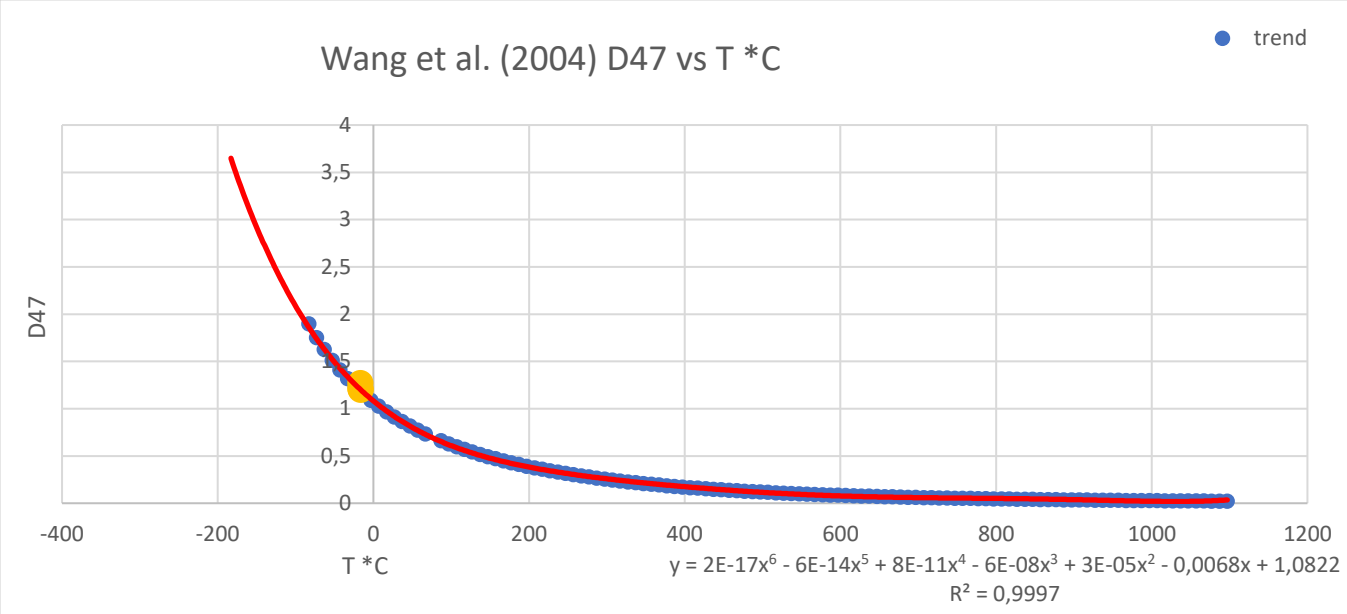


*Graph 3: D47 vs T*C values of Wang et al. (2004) (blue) with a derived trendline by performing a 6th order polynomial regression ($D47 = 2E\text{-}17(T°C)^6 - 6E\text{-}14(T°C)^5 + 8E\text{-}11(T°C)^4 - 6E\text{-}08(T°C)^3 + 3E\text{-}05(T°C)^2 - 0{,}0068(T°C) + 1{,}0822$) on the data points ($R^2 = 0.9997$). This Trendline will be used to solve the temperature – D47 relationship in an absolute reference frame proposed by wang et al., (2004). Final results for the samples are indicated in Yellow and correspond to a temperature of about -16°C.*

| Source (in Dennis et al., 2011) | Slope | Intercept | ETF |
|---|---|---|---|
| Harvard University | 1.0105 | 0.9539 | (1) D47 = 1.1548x - 0.9343 |
| Yale University | 1.0630 | 0.9227 | (2) D47 = 1.0630x - 0.9227 |
| John Hopkins University | 1.0303 | 0.9194 | (3) D47 = 1.0303x - 0.9194 |
| California Institute of Technology | 1.1548 | 0.9343 | (4) D47 = 1.1548x - 0.9343 |
| Utrecht University | 1.0517 | 0.9464 | (5) D47 = 1.0517x - 0.9464 |
| This Study | 0.7738 | 0.6893 | (6) D47 = 0.7126x - 0.6327 |

*Table 7: Overview of ETF functions. For a more detailed overview Dennis et al. (2011) has presented a thorough analyses. The ETF functions displayed in this table have a negative intercept value, whilst the ETF functions presented by Dennis et al. have a positive intercept value. This makes no difference regarding the temperature calibration, and will not be further elaborated upon.*

Wang et al. (2004). Hereafter the Initial D47 values of the Samples will be plotted against the D47 values of Wang et al. (2004) and finally, fitted to an extrapolated D47 vs T°C curve.

The generally accepted values of $CO_2$ for D47 given by Wang et al. (2004) have been presented in Table 6, along with D47 values obtained through measurements of two standard gasses by IRMS measurements, and values for D47 measured by colleagues for heated gasses. Using the values displayed in Table 6, several (two) ETF functions are created and displayed in Graph 1.

By taking the values measured for D47 by Wang et al. (2004) as ground truth to Calibrate the D47 measured In Other laboratories. Doing this gives us a series of ETF functions, to which the measured D47 values for samples are projected. A compilation of ETF functions is listed in Table 7. for a more detailed inquiry in the accuracy and determination of these ETF functions, a very thorough analysis is presented by Dennis et al. (2011). This gives a range of possible temperatures and hence by applying a geothermal gradient, the source depth of origin of the atmospherically venting $CO_2$.

As Can be noted by the ETF generated from the measured Standards processed through the cryogenic $CO_2$ purification set-up, (ETF_W_vs_B in Graph 2, and "this study" in Table 7) the slope and the intercept values vary significantly as opposed to ETF functions presented by D47 Analyses of $CO_2$ in other Laboratories. This can be (1) due to re-equilibration of

| DILUTED SAMPLES | AVG. D47 | D47 WANG ET AL., (2004) EQUIVELANT VALUES | AVG. D47 ST.DEV | AVG. D47 SE | AVG. D13C | AVG. D13C ST.DEV | AVG. D18O | AVG. D18O ST.DEV | T*C [ETF] | N |
|---|---|---|---|---|---|---|---|---|---|---|
| **LATERA 2 DIL** | 0,410 | 1.212 | 0,073 | 0,028 | 0,464 | 0,009 | 1,864 | 0,020 | -16,5 | 1 |
| **S.VITT 6B DIL** | 0,369 | 1.199 | 0,048 | 0,017 | -3,146 | 0,032 | 0,984 | 0,021 | -16,2 | 1 |
| **AILANO 2 DIL** | 0,479 | 1.272 | 0,116 | 0,057 | 0,726 | 0,086 | 2,888 | 0,101 | -16,7 | 1 |

*Table 8: Averaged results of first cycle of measurements using set-up 1. The ETF functions are used (graph 1 & 2) to recalculate the new Δ47 values to be plotted against the temperature in an absolute reference frame by wang et al., (2004).*

the clumped signal within the steel cylinder which was made approximately a week prior to measurements. A difference in slope and intercept can also be explained by (2) a high degree of partial refractionation of the δ47 clumped isotopic $CO_2$ signal occurring within the cryogenic $CO_2$ purification measurement set-up during the purification cycle. Another possibility is that (3) during the preparation of the stainless-steel cylinder containing the heated reference gas, the vacuum integrity of the offline vacuum-line was compromised with the breakage of the Quartz cylinder, releasing the $CO_2$ with the clumped signal of 1000*C. Finally, (4) the $CO_2$ filled within the reference bellow of the IRMS unit has a higher clumped signal than initially measured. Out of these four possibilities, a compromise in the off-line vacuum during the preparation of the heated cylinder, could greatly influence the clumped D47 signal of the heated $CO_2$. Any degree of atmospheric contamination can lead to much higher values than can be expected for $CO_2$ gas equilibrated at 1000*C. A combination of the four mentioned causes could also be plausible.

Because there is such a great difference between the ETF function calculated from the processed reference gasses during the measurements cycles, and the ETF functions presented by Laboratories around the globe, it has been decided to use all ETF functions for the measured D47 values from $CO_2$ derived from the sampled venting gasses. Using all ETF's the D47 will be calculated standardized to Wang et al.'s presented values for D47. This will give a possible range of D47 values, which can in turn be converted to temperature values by using Wang et al.'s (2004) calibration curve established for temperature. This temperature calibration curve has been created by performing a logarithmic regression analyses on the D47 vs T*C relationship measured. The Wang et al (2004) Temperature calibration curve is presented in graph 3.

**Initial results samples:**

By looking at the initial results for the processed samples it can be observed that for successful measurements a dilution of the original acquired air sample was necessary when using processing method 1 (Figure 7). The majority measurements either failed because (1) the pressure difference between the bellows was too large to compensate by the IRMS, or, (2) the calculated standard deviation is higher than the maximum accepted 0.04‰. A thorough analyses of the initial results will be performed in the discussion chapter of this report to resolve the initial observations.

Using the polynomial function derived from T*C vs D47 presented Wang et al. (2004) (graph 3) The initial results for D47 measured on $CO_2$ from the samples can be plotted to fit on the temperature curve. The temperature values for the samples for the measured samples have been displayed in Table 8. Since the derived ETF function, and the calculated initial temperatures differ greatly from what has been expected, a thorough analyses is necessary to attempt to resolve these discrepancies. An extensive analysis of the logs has been performed to calibrate the equipment to the air samples introduced. This will be discussed in the discussion chapter of this report. Furthermore, an Empirical transfer function and N2O correction are still needed to finalize data analyses, however an analyses of the measurement logs is needed before this.

| | |
|---|---|
| **Total amount of processed purified $CO_2$ samples** | 63 |
| Total amount of sample measurements of $CO_2$ performed on mass spectrometer | 44 |
| Total amount of processed reference gasses (standards) | 19 |
| Total amount of processed standards meeting criteria #1 | 17 |
| Total amount of processed standards meeting criteria #1 & #2 | 17 |
| Total amount of processed standards meeting criteria #1, #2 & #3 | 13 |
| Total amount of processed standards meeting criteria #1, #2, #3 & #4 | 4 |
| Total amount of processed standards meeting all criteria | 3 |
| Total amount of processed samples | 25 |
| Total amount of processed samples meeting criteria #1 | 24 |
| Total amount of processed samples meeting criteria #1 & #2 | 24 |
| Total amount of processed samples meeting criteria #1, #2 & #3 | 0 |
| Total amount of processed samples meeting criteria #1, #2, #3 & #4 | 0 |
| Total amount of processed samples meeting all criteria | 0 |
| | |
| **Rate of successes:** | |
| Mass spectrometer software | 70% |
| Cooling or heating | 72% |
| Pressure equalization between reference and sample bellow | 18% |
| Mislabeling of measurements | 68% |
| Total success rate | 3% |

*Table 9: Overview of log statistics and statistical evaluation of success rate.*

**Discussion:**

**Statistical evaluation measurement cycles**

Since the processing the samples using method 1 (**Figure 7**) have failed to produce consistent reliable and accurate measurements on the mass spectrometer regarding the d47 clumped $CO_2$ signal for the obtained samples (Table 5, 6, 7 & 8), it is necessary to perform a detailed analysis on the cause of these failed measurements to propose a more viable method for processing the obtained air samples. It has been determined that an accurate measurement has to meet the following criteria:

1. Successful heating to 240*C, and cooling to -20*C of the GC column
2. Successful cyclical freezing and thawing of purified $CO_2$ by using liquid nitrogen.
3. An expected d47 value lower than the room temperature standard d47 value, and higher than the 1000*C heated standard d47 value.
4. 8 measurement cycles with equalized pressure between sample and reference bellow on the mass spectrometer.
5. A Standard deviation smaller than 0.04‰ for the measured d47 values

By comparing the sensor logs from the $CO_2$ purification set-up (Appendix 4A) to the output logs of the mass spectrometer (Appendix 4B), the relationships between the two devices is analysed. The results are displayed below in Table 9.

From the statistical analyses, it can be observed that the factor of greatest influence resulting in failed measurements is the unequal pressure difference between the sample and reference bellow within the mass spectrometer. furthermore, the Easotope software and the heating and cooling of the oven are deemed the greatest factors of influence respectively contributing to a failed measurement. The main identified source of failure, the pressure equalization problems, is analysed thoroughly to determine the cause of the unequal pressure problems occurring inside the IRMS. This is done by cross comparison and trend analyses of the measurement logs.

**Trend analyses from measurement logs**

In order to calibrate the processing equipment in use, an extensive analyses of the measurement logs are performed and displayed in the graphs below (Graph 4,5 & 6). Using the sensor telemetry data, relationships between variables can be explored for causal relationships by fitting curves through the plotted logged data points. These relationships, or absence

thereof, are used to evaluate the causes of failed measurements using processing method 1.

**Graph 4** shows the averaged intensity measured for m/z=44 for the reference and sample bellow in the mass spectrometer. The trendline shows a significant linear relationship present. This makes sense since the mass spectrometer can only perform accurate measurements when the difference in pressure between the sample and reference bellow are below 300 mV. The upper and lower limit are indicated by the trendlines y=Trendline-300 (Yellow) & y=Trendline+300 (green) respectively. It can be observed that the measurements corresponding to the processed air samples (purple data points) are located outside the range for an accurate measurement. The pressure of the sample bellow is too low compared to the pressure in the reference bellow, which fails to adjust its pressure to the sample bellow, leading to a failed measurement. The below the acceptable bounds

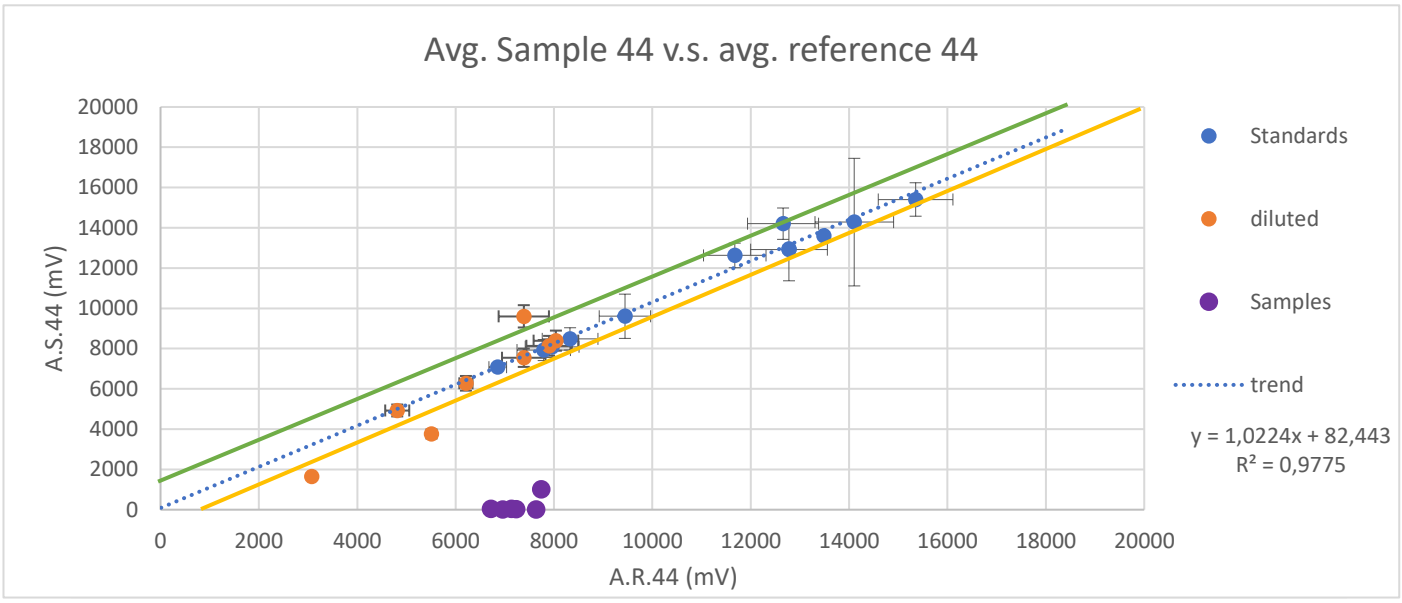


*Graph 4: Intensity sample m/z=44 vs. intensity reference m/z=44. Note that the samples do not coincide with the trendline for measured standards. Error bars = 1 St.dev. The green solid line indicates the largest acceptable offset between sample 44 and reference 44. The yellow solid line indicates the lowest acceptable offset in measured intensity on sample 44 and reference 44.*

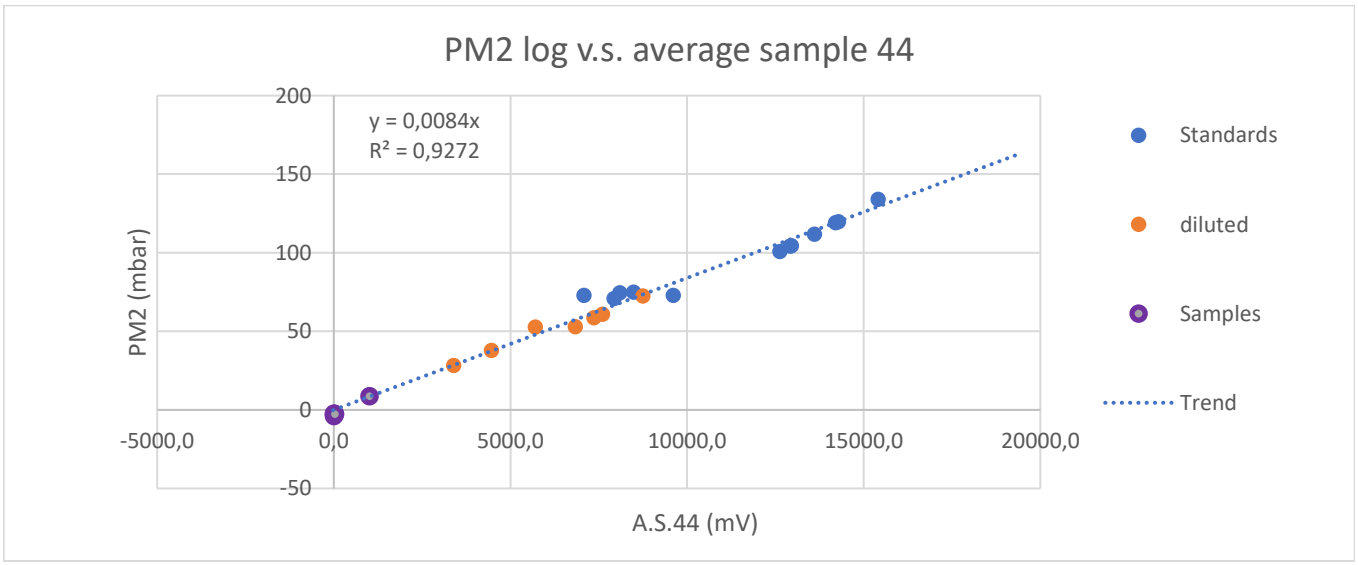


*Graph 5: PM2 (mbar) vs. intensity measured on sample bellow gas on m/z=44. For all data points, a relationship clearly is present between the PM2 log and the averaged Intensity of the sample m/z=44.*

intensity measured of the sample bellow, is due to the fact that too little purified $CO_2$ is introduced into the mass spectrometer for measuring. When looking at the results for all the processed data in graph 4, it can be noted that for the measured standard gasses, the sample bellow and reference bellow had no major problems adjusting to the required equal pressure. These observations require further analyses to indicate a reason for the deviation of the measured samples from the trend derived from the processed reference gasses. To achieve that, the PM2 pressure response is plotted against the average intensity for m/z=44 measured on the sample bellow, in order to investigate the relation between the pressure measured for purified $CO_2$ vs. the intensity measured on m/z=44 for the sample gas bellow (**Graph 5**). The PM2 is a pressure sensor located at the end of the cryogenic purification set-up. This pressure sensor shows an increasingly positive pressure response with an increasing quantity of purified $CO_2$. PM2 is thus the best indicator to check the quantity of $CO_2$ at the end of the cryogenic $CO_2$ purification process. It can be observed from graph 5 that there is a strong correlation between the pressure response of PM2 and the intensity on m/z=44 measured on the sample gas using the IRMS. All data points correlate significantly with the derived trendline, which confirms that measuring the pressure response on PM2 is a good indicator to significantly predict the intensity of m/z=44 measured on the mass spectrometer for the sample bellow. It can thus definitively be stated that the PM2 pressure represents the amount of purified $CO_2$ gas injected for measurement the mass spectrometer. It can also be observed that the purified $CO_2$ derived from the air samples has a low-pressure response on PM2 (Graph 5, purple data points), leading to a low intensity on m/z=44. Under ideal circumstances an accurate measurement has an intensity of 10.000 mV, or higher, measured on m/z=44 as observed in graph 5. This correlates with a pressure higher then 80mbar measured on PM2. This relation will be explored by plotting the PM2 log against the calculated amount of $CO_2$ injected into the $CO_2$ purification set-up (Graph 6), calculated and displayed in table 4.

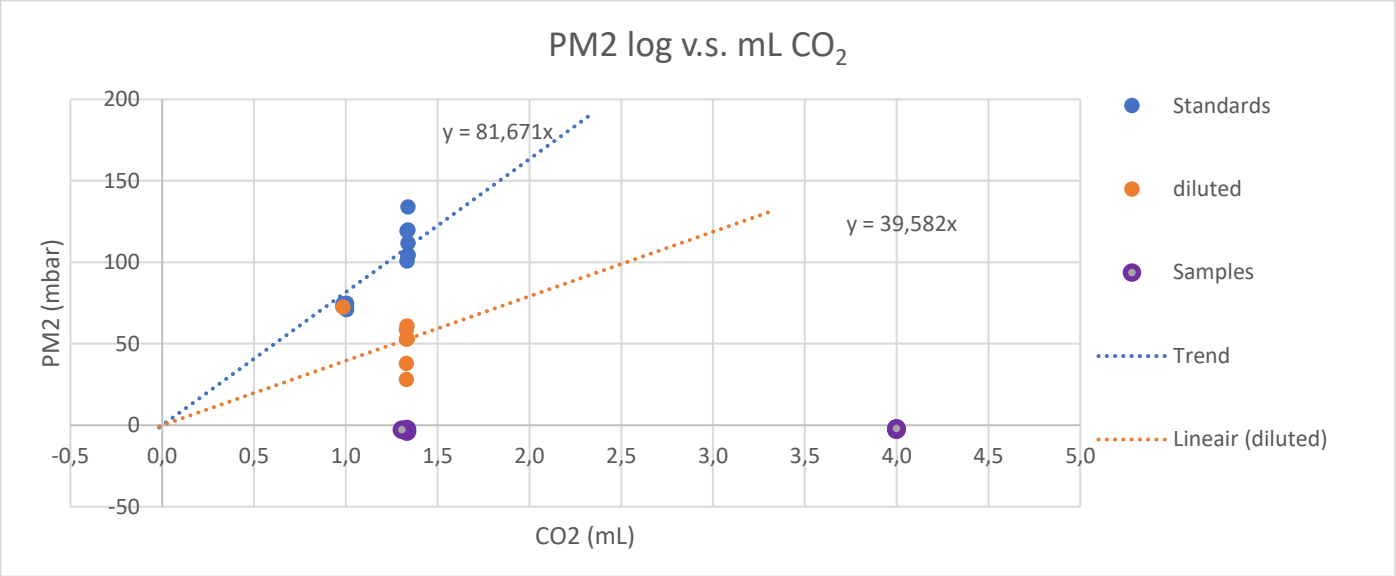


*Graph 6: PM2 (mbar) vs. $CO_2$ input calculated by using $CO_2$ concentration values from Table 4. Note the absence of a correlation between the calculated $CO_2$ input, and the PM2 response.*

Graph 6 shows the absence of a correlation between the processed air samples (purple) and the pressure response measured on PM2. This can mean that either (1) the measured $CO_2$ concentrations of the sample gas are too high, or, (**2**) the $CO_2$ purification set-up is not 100% efficient in processing samples of different $CO_2$ concentrations, caused by the loss of sample gas within the purification set-up. It is the most likely that using method 1 for accurate analyses for the sample gas is impossible due to an insignificant correlation between the amount of sample injected into the purification set-up, and the pressure response measured on PM2. Further indication for the validity of this statement is observed by plotting linear trendlines for the processed standards and the processed diluted samples. A Trendline for the acquired air samples is not possible since the PM2 log does not show a significant response to amount of $CO_2$ injected into the purification set-up. The trendline for the processed reference gasses has a slope of about 82 mBar per mL of $CO_2$ injected in the cryogenic purification set-up. The trendline for the processed diluted samples has a slope of about 40 mBar per mL $CO_2$ injected in the cryogenic purification set-up. Looking at table X, where the $CO_2$ concentration is presented in % for samples, standards

and diluted samples, it can be observed that the diluted samples have a $CO_2$ concentration of about 0.4%, whilst the reference gasses have a $CO_2$ concentration of about 0.04%. correlating these observation gives a significant relation between the $CO_2$ concentration of the injected sample, and the expected pressure response measured on PM2 (See Appendix 2D).

*"for every factor 10 increase in* $CO_2$ *concentration of the to measure sample compared to the* $CO_2$ *concentration of the reference gasses, a factor 2 decrease in pressure response is measured on PM2".*

The above statement illustrates that there is a significant scaling issue with regards to measurements performed on samples with higher concentrations of $CO_2$. The processed standards have the equivalent of ambient concentrations of CO2 in the range of 300-500 PPM (0.03-0.04%). Method 1 (figure 7), the chain-linked processing set-up, had previously been constructed to measure deviations for $CO_2$ on the d47 clumped signal in ambient air. Using the same method and workflow for higher $CO_2$ concentration samples induces purification efficiency problems within the cryogenic purification set-up. Assuming the ambient concentrations of Co2 are processed with a 100% efficiency, it can be deduced with the statement above that processing the obtained air samples with higher $CO_2$ concentrations leads a purification efficiency of 5%. It was initially calculated to inject 1.33 mL of purified $CO_2$ derived from the sample into the mass spectrometer sample bellow for measurement. Since higher concentrations lead to a purification efficiency of 5% it can be determined that only 0.07mL of purified $CO_2$ is injected into the mass spectrometer for measurement. This can be observed by the lack of a pressure response measured on PM2 for the high concentration air samples in graph 4. Because of the scaling issues with processing high $CO_2$ concentration samples, all measurements performed have failed by debunking the assumption that the cryogenic purification set-up is capable to process all injected samples with varying $CO_2$ concentrations equally efficient. Correcting for unequal processing efficiency problems is not possible and leads to the unequal treatment of processed samples. Elaborate testing of cryogenic processing set-up sensitivity to injecting varying concentrations of $CO_2$ is therefore needed.

In the absence of a more diverse group of heated refence gasses, there are only two calibration points at 25°C and 1000°C for reference of the measured D47 clumped isotope signal obtained from the air samples. A more prudent approach to the analyses of D47 measured from subsurface originating venting $CO_2$, is to focus on creating multiple accurate calibration points for higher temperatures. Since the majority of research on clumped isotopes focuses on the analyses of D47 to indicate its paleotemperature at the moment of deposition, the majority of the D47 standards found in literature focus on the temperature range between 50°C and 0°C. Since this is unbroken ground, the focus should have been laid on creating accurate reference standards for higher temperature ranges, followed by the purification and measurement of the acquired air samples. This leads to the identification of a possible limitation on the usage of D47 isotopologues measured on CO2 leaking from a subsurface source. Using Δ47 as an indicator of the source of depth might be held to a certain limited, since the equilibration speed with water (reactions 2 & 3) could be very high considering the observed trend of increasing equilibration reaction speeds, if these trends hold true when extrapolated to subsurface condition reflecting the range of 100-400°C. Therefore, for the purpose mitigating hazardous conditions concerning onshore CCS by using Δ47 as an indicator to determine the depth of the source origin of CO2 in the subsurface with the goal to monitor for $CO_2$ leakage, is doubtfull to be feasible. However, this is just an hypothesis on made on the observed trend of Clog et al., (2015)'s results concerning an increasing isotopologue exchange rate for D47 at increasing temperatures.

Adding more uncertainty to the identified scaling issue is the fact that upon closer inspection, the GC column is probably unable to completely purify the sample $CO_2$. This is because the Porapak mesh (Q80) within the GC column is unable to filter sulphide components from the injected mixture of sample gasses. This is confirmed by a strong smell of rotten eggs at the end of the purification process where it should not be present. Due to the high sensitivity of the temperature sensors involved in heating and cooling the GC oven, many times it had occurred that the GC column was heated or cooled beyond what its operating conditions, probably damaging the GC column or the liquifying the Porapak mesh in the process. This could also have simply been avoided by inquiring about the operating status of the cryogenic processing set-up, performing a maintenance check of all components before measuring in a time intensive schedule and finally to check the inventory for replacement parts if a crucial part fails.

**Conclusion:**

In conclusion, the clumped d47 isotopic signature measured from naturally leaking $CO_2$ from subsurface, is unlikely to be a relevant application for $CO_2$ monitoring for increasing CCS safety. The reaction rates of $CO_2$ equilibration with (ground) water in subsurface conditions, could distort the true δ47 because of isotopologue exchange. By using the the chain-linked cryogenic purification set-up (method 1), this could not be proven or disproven. The measurements using the IRMS have not given any useable results since the final temperatures indicate a source temperature of around -16°C, for all measured samples. The possibility of the δ47 equilibrating with groundwater, before venting at surface levels is a very likely possibility. However, with the data acquired and the analyses performed this can also not be proven or disproved. Using method 1 for processing the obtained air samples gave erroneous measurements because (1) too little purified sample $CO_2$ is injected into the sample bellow of the mass spectrometer due to purification efficiency loss of higher concentration $CO_2$ samples. this resulted in an unbridgeable pressure difference in the IRMS, leading to a sequence of failed measurements. Analyses of the sensor logs shows that for samples with higher concentrations of, the $CO_2$ purification set-up is unable to effectively purify all the $CO_2$ introduced into the $CO_2$ purification set-up, with leakages and large quantities of sample lost. For high $CO_2$ concentrations, the amount of purified sample injected into the mass spectrometer for measurement is therefore always much lower than initially determined. This quantitative discrepancy inevitable leads to a failed measurement due to pressure equalization problems which cannot be solved using method 1. Thus, for any sample introduced into the cryogenic $CO_2$ purification set-up with a higher than ambient concentration of CO2 (300-400 PPM), a processing efficiency scaling issue has been identified for determining the quantity of $CO_2$ injected into the mass spectrometer sample bellow for δ47 clumped signal measurements. To compensate for the unpredictable quantity of $CO_2$ purified by the $CO_2$ purification set-up processing, an unchained processing method has been proposed based on Method 1. This method has the extra benefit of (1) manually being able to control the quantity of $CO_2$ injected into the mass spectrometer for measurement, which ensures an equalized pressure between the mass spectrometer's sample and reference bellow. Also, (2) the processed samples can be captured and stored for measurement at a later moment on the mass spectrometer. Finally, (3) by ridding the $CO_2$ purification set-up from inefficiencies identified within the liquid nitrogen refilling system and decreasing the diameter of the connection to the oven housing the GC column, it is less likely that the liquid nitrogen vessel is emptied during cryogenic processing which otherwise would have resulted in a failed measurement. These adaptations are an improvement, but not an ideal solution to the experienced problems. Within the $CO_2$ purification set-up use is made of long vacuum lines with varying diameters which, results of fractionation of the δ47 clumped $CO_2$ signal within the $CO_2$ purification system. This phenomenon can be mediated by using shorter vacuum lines, with a single diameter, minimizing the amount of isotopic fractionation occurring. Furthermore, a close inspection of the GC column with porapak filling is needed, since the GC column built in the $CO_2$ purification set-up is unable to separate some pollutants present within the air samples ($H_2S$), resulting in anomalous clumped signatures measured for δ47.

**Summary:**

measuring the clumped $CO_2$ signal on d47 for samples obtained from naturally leaking $CO_2$ from subsurface sources, to identify the possible temperature and hence depth of the source of origin, could not be accomplished due to an identified scaling issue regarding the cryogenic purification of high concentration $CO_2$ samples. It cannot be concluded from the measurement IRMS results whether analysing δ47 clumped signals from $CO_2$ from subsurface sources is a good indicator for determining the source depth of leakage. The subject remains open for debate.

**References:**


Affek H. P. and Eiler J. M. (2006) Abundance of mass 47 CO2 in urban air, car exhaust, and human breath. Geochim. Cosmochim. Acta 70, 1–12.

Affek H. P., Xu X. M. and Eiler J. M. (2007) Seasonal and diurnal variations of 13C18O16Oin air: initial observations from Pasadena, CA. Geochim. Cosmochim. Acta 71, 5033–5043.

Affek H. P., Zaarur S. and Douglas P. M. J. (2009) Mass spectrometric effects on 'clumped isotopes' calibration. Geochim. Cosmochim. Acta 73, A15.

Affek H.P. (2013). CLUMPED ISOTOPIC EQUILIBRIUM AND THE RATE OF ISOTOPE EXCHANGE BETWEEN CO2 AND WATER, American Journal of Science, Vol. 313, April, 2013, P. 309–325.

Barberi, F., F. Innocenti, P. Landi, U. Rossi, M. Saitta, R. Santacroce, and I. M. Villa (1984), The evolution of Latera caldera (central Italy) in the light of subsurface data, Bull. Volcanol., 47(1), 125 – 141.

Barberi, F., et al. (1994), Plio-Pleistocene geological evolution of the geothermal area of Tuscany and Latium, Mem. Descr. Carta Geol. Ital., 49, 77 – 134.

Belluomini G., Branca M. & Delitala L. (1984), Isoleucine epimerization ages of some Pleistocene sites near Rome, HUMAN EVOLUTION Vol. 1 - N. 3 (209-213).

Bertrami, R., G. M. Cameli, F. Lovari, and U. Rossi (1984), Discovery of Latera geothermal field: Problems of the exploration and research, paper presented at Seminar on Utilization of Geothermal Energy for Electric Power Production and U. N. Econ. Comm. for Eur., Florence, Italy.

Centamore, E., and Nisio, S., 2003, Effects of uplift and tilting in the Central-Northern Apennines (Italy), Quaternary International, 101-102:93-101.

Chiodini, G., C. Cardellini, A. Amato, E. Boschi, S. Caliro, F. Frondini, and G. Ventura (2004a), Carbon dioxide Earth degassing and seismogenesis in central and southern Italy, Geophys. Res. Lett., 31, L07615.

Chiodini, G., A. Baldini, F. Barberi, M. L. Carapezza, C. Cardellini, F. Frondini, D. Granieri, and M. Ranaldi (2007), Carbon dioxide degassing at Latera caldera (Italy): Evidence of geothermal reservoir and evaluation of its potential energy, J. Geophys. Res., 112, B12204.

Eiler, J. M., and Schauble, E., (2004), 18O13C16O in Earth's atmosphere: Geochimica et Cosmochimica Acta, v. 68, n. 23, p. 4767–4777.

Affek H.P. (2013), Clumped isotopic equilibrium and the rate of isotope exchange between CO2 and water. Amircan Journal of Science, 313 (4), pp. 309-325.

Clog M. , Stolper D., Eiler J.M. (2015), Kinetics of CO2(g)–H2O(l) isotopic exchange, including mass 47 isotopologues, Chemical Geology, 395, pp. 1-10.

ENOS newsletter may 2017

J. Dennis, Kate & Affek, Hagit & H. Passey, Benjamin & P. Schrag, Daniel & M. Eiler, John. (2011). Defining an absolute reference frame for 'clumped' isotope studies of CO2. Geochimica et Cosmochimica Acta. 75. 7117-7131.

Ghosh P., Adkins J., Affek H., Balta B., Guo W. F., Schauble E. A., Schrag D. and Eiler J. M. (2006) 13C–18O bonds in carbonate minerals: a new kind of paleothermometer. Geochim. Cosmochim. Acta 70, 1439–1456.

Giustini F., Micheala B., Brilli M., Lombardi S., Voltarttorni N., Widory D., (2013). Determining the origin of carbon dioxide and methane in the gaseous emissions of the San Vittorino plain (Central Italy) by means of stable isotopes and noble gas analysis Applied Geochemistry 34 (2013) 90–101.

Guo W. F., Mosenfelder J. L., Goddard W. A. and Eiler J. M. (2009) Isotopic fractionations associated with phosphoric acid digestion of carbonate minerals: insights from first-principles theoretical modeling and clumped isotope measurements. Geochim. Cosmochim. Acta 73, 7203–7225.

Hofmann M.E.G., Pons T.L., Ziegler M., Lourens L.J. and Röckmann T. Fractionation of clumped isotopes of CO2 during photosynthesis. Unpublished manuscript (expected publication 2017).

Huntington K. W., Eiler J. M., Affek H. P., Guo W., Bonifacie M., Yeung L. Y., Thiagarajan N., Passey B., Tripati A., Daeron M. and Came R. (2009) Methods and limitations of 'clumped' CO2 isotope (D47) analysis by gas-source isotope ratio mass spectrometry. Journal of Mass Spectrometry 44, 1318–1329.

Mariucci M.T., Montone P., Pierdominici S.,(2008). Active stress field in central Italy: a revision of deep well data in the Umbria region, Ann. Geophys., 51 (2–3), pp. 433 –442..

Passey B. H., Levin N. E., Cerling T. E., Brown F. H. and Eiler J. M. (2010) High-temperature environments of human evolution in East Africa based on bond ordering in paleosol carbonates. Proc. Natl. Acad. Sci. USA 107, 11245–11249.

Schauble E. A., Ghosh P. and Eiler J. M. (2006) Preferential formation of 13C–18O bonds in carbonate minerals, estimated using first-principles lattice dynamics. Geochim. Cosmochim. Acta 70, 2510–2529.

Wang Z. G., Schauble E. A. and Eiler J. M. (2004) Equilibrium thermodynamics of multiply substituted isotopologues of molecular gases. Geochim. Cosmochim. Acta 68, 4779–4797.

**List of Figures. Tables, Graphs & Appendices:**

Appendix 1: Alterations to chained processing setup creating alternative method 2
Appendix 2A: Isodat raw data extraction macro
Appendix 2B: Microsoft Excel raw data filtering sheet
Appendix 2C: Microsoft Excel formulae sheet
Appendix 2D: Overview of initial result using processing method 1
Appendix 3: N2O correction sheet
Appendix 4A: Compilation of output logs mass spectrometer
Appendix 4B: Compilation of output logs cryogenic processing set-up

**Acknowledgements:**

A special thank you is in order for TNO, the host company of the author's internship with emphasis on dr. T.V. Goldberg, for her contribution and guidance on this project, dr. M.E.G. Hoffmann for instruction and lending out her equipment, dr. M. Ziegler for his efforts, A.E van Dijk for giving a helping hand in the laboratory, PhD candidate A.E. van der Meer for her help on the ETF analyses, and finally, dr. S.E. Bienbeau for his experience and knowledge of the Italian plains. A final token of appreciation goes out to dr. D. Paul & dr. C. van der Veen of the IMAU institute for being flexible and patient, giving clarity in time of need.